Chinese Chemical Letters 34 (2023) 108620

Contents lists available at ScienceDirect

Chinese Chemical Letters

journal homepage: www.elsevier.com/locate/cclet

Constructing cactus-like mixed dimensional MOF@MOF as sorbent for extraction of bisphenols from environmental water

Peige Qin[a], Shiping Zhu[a], Mengyao Mu[a], Yanmei Gao[a], Zongwei Cai[b], Minghua Lu[a,*]

[a] Henan International Joint Laboratory of Medicinal Plants Utilization, School of Chemistry and Chemical Engineering, Henan University, Kaifeng 475004, China

[b] State Key Laboratory of Environmental and Biological Analysis, Department of Chemistry, Hong Kong Baptist University, Hong Kong 999077, China

ARTICLE INFO

Article history:
Received 16 February 2023
Revised 25 May 2023
Accepted 25 May 2023
Available online 27 May 2023

Keywords:
PCN-134@Zr-BTB composite
Metal-organic frameworks (MOFs)
Mixed-dimensional
Dispersive solid-phase extraction
Endocrine disrupting compounds (EDCs)
High-performance liquid chromatography

ABSTRACT

Metal-organic frameworks (MOFs) received considerable attention to adsorption and removal of various environmental pollutants because of some inherent advantages. However, it is challenging but meaningful to design and fabricate hierarchical mixed-dimensional MOFs with synergistic effects to enhance the performance for removal and preconcentration of environmental pollutants. Herein, a new hierarchical two-dimensional (2D)-three-dimensional (3D) mixed-dimensional cactus-like MOF@MOF hybrid material (PCN-134@Zr-BTB) was prepared by *in-situ* growth of 2D MOF nanosheets (Zr-BTB) on the surface of 3D MOF (PCN-134). The PCN-134@Zr-BTB composites combine the advantages of 2D and 3D MOFs with extensive mesoporous structures and large surface area for effective removal and enrichment of bisphenols (BPs). In comparison with pristine PCN-134 and Zr-BTB materials, the PCN-134@Zr-BTB hybrid material presented excellent adsorption performance for BPs. The adsorption isotherms are consistent with the Langmuir model, and the maximum adsorption capacity of four bisphenols (BPs) ranged from 135.1 mg/g to 628.9 mg/g. The adsorption kinetics are in accordance with the pseudo-second-order model. The recoveries ranged from 72.8% to 108%. The limits of detection were calculated at 0.02–0.03 ng/mL. The enrichment factors were calculated in the range of 310–374. According to FT-IR and XPS analysis, the main adsorption mechanisms are hydrogen bonding and π-π stacking. Nevertheless, this work provides a new and convenient strategy for the preparation of new hierarchical mixed-dimensional MOF@MOF (PCN-134@Zr-BTB) hybrid material for extraction and enrichment of BPs from aqueous matrix.

As one of environmental endocrine disruptors, bisphenols (BPs) are extensively used in industrial and consumer products, such as coatings, membrane materials, packaging materials and other daily necessities [1]. With widespread use of BPs throughout the world, they are commonly existed in environmental sample (*e.g.*, wastewater and river sediments), human urine and food samples [2]. BPs can cause a broad range of adverse effects including reproductive system disorders, neurobehavioral disorders, cardiovascular and immune diseases on animals, humans and aquatic organisms even at low concentrations [3,4]. Therefore, the removal of BPs from environmental samples and their sensitive detection have attracted a growing interest.

Various materials including carbon nanotube [5,6], carbon nitrite [7], metal-organic frameworks (MOFs) [8–10], covalent organic frameworks [11,12] and porous organic polymers [13,14] have been designed to extract and preconcentrate environmental pollutants. Among them, MOFs received tremendous attention because of their large surface area, high adsorption capacity, excellent chemical/thermal stability, controllable pore size and plentiful active sites [15]. MOFs usually consist of three-dimensional (3D) structure and two-dimensional (2D) nanosheet [16]. Many 3D MOFs have been utilized for removal of BPs from water [17–19]. 2D MOF not only has the merits of 3D MOF, but also can offer high surface area and abundant accessible adsorption sites [20–22]. However, the application of 2D MOFs as sorbents remains great challenges because most 2D MOFs are ultra-light materials, which result in difficult to recover from suspensions with high-speed centrifugation during adsorption [23].

Currently, the hierarchical mixed-dimensional 2D-3D MOF@MOF composites received tremendous consideration because of some inherent advantages over pristine monomeric MOFs, such as excellent adsorption performance because of synergistic effect [24] and easy separation of 2D-MOF ultra-light materials from solution [25]. In this work, the hierarchical 2D-3D MOFs composites with cactus-like structure was prepared and used as sorbent for

* Corresponding author.
E-mail address: mhlu@henu.edu.cn (M. Lu).

https://doi.org/10.1016/j.cclet.2023.108620
1001-8417/

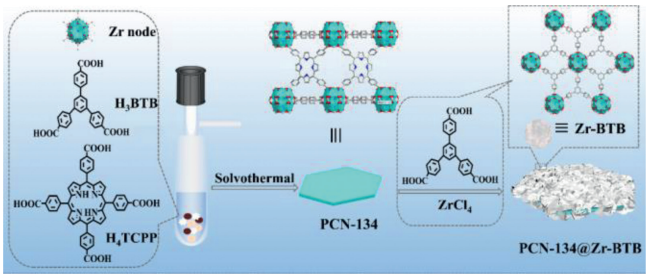

Fig. 1. Schematic of the preparation processes of PCN-134@Zr-BTB.

extraction of BPs from environmental water. As shown in Fig. 1, the 3D PCN-134 was synthesized through a simple solvothermal method [26]. Then, the PCN-134@Zr-BTB hybrid material was prepared by *in-situ* growth of 2D Zr-BTB nanosheets on the surface and edges of 3D PCN-134 nanoplates. The structure and morphology of PCN-134@Zr-BTB were systematically investigated by a series of characterization techniques. Then, the prepared PCN-134@Zr-BTB was used as adsorbent for removal and enrichment of bisphenols including bisphenol F (BPF), bisphenol A (BPA), bisphenol B (BPB), bisphenol AF (BPAF) (chemical structures are shown in Fig. S1 in the Supporting information) from environmental water. The parameters affecting the extraction performance were optimized in detail. Furthermore, the adsorption isotherm and adsorption kinetics were conducted to explore the adsorption mechanism.

According to literature, the addition of water as catalyst can significantly affect the layer thickness of Zr-BTB material [27], which may have an impact on the specific surface area and extraction performance of the materials. Therefore, Zr-BTB materials with different layer thicknesses (Zr-BTB-x) were synthesized through adding different volume of water (0, 0.5, 1.0, 2.0 and 2.5 mL). The detailed preparation processes were shown in Supporting information. The obtained materials were recorded as Zr-BTB-0, Zr-BTB-0.5, Zr-BTB-1.0, Zr-BTB-1.5, Zr-BTB-2.0 and Zr-BTB-2.5. The layer thickness, morphology, structure and extraction performance of Zr-BTB-x material were studied. The detailed results and respective figures (Figs. S2 and S3 in Supporting information) were provided in Supporting information. Experimental results demonstrated that the maximum extraction peak areas and adsorption capacities for target BPs were obtained with Zr-BTB-1.5. Therefore, Zr-BTB-1.5 was employed for fabrication of PCN-134@Zr-BTB composites.

The structures of PCN-134, Zr-BTB-1.5 and PCN-134@Zr-BTB were examined by X-ray diffraction (XRD). The XRD pattern of PCN-134 (Fig. S4 in Supporting information) was in agreement with previous study. As demonstrated in Fig. 2a, it is difficult to distinguish the two components in the PCN-134@Zr-BTB composite due to the overlapping of main diffraction peaks of PCN-134 (5.23°) and Zr-BTB (5.1°) in the hybrid material. However, the intensity of (010) plane in composite has a significantly increase compared to that of pristine PCN-134 nanoplate, further validating the successful synthesis of the PCN-134@Zr-BTB hybrid materials (Fig. 2a). The FT-IR spectra of those materials are shown in Fig. 2b. The spectrum of PCN-134@Zr-BTB displayed an additional adsorption band at 972 cm^{-1} compared to that of Zr-BTB, which was attributed to the deformation vibration of the N–H bond on the H_2TCPP pyrrole ring. The band at 1542 cm^{-1} can be imputed to C=C stretching vibration. The vibration peak at 1658 cm^{-1} can be concluded as the stretching vibration of C=O of carboxylic acid in TCPP or BTB. The peak near 1595 cm^{-1} and 1413 cm^{-1} represent -(C–O–C)- bonds. The peak of 478–800 cm^{-1} owed to the deformation vibration of Zr-O/Zr-OH. The bands at 2929 cm^{-1} and 3058 cm^{-1} are attributed to the C–H vibration stretching. The band around 3500 cm^{-1} indicated the existence of OH and/or H_2O groups in all the prepara-

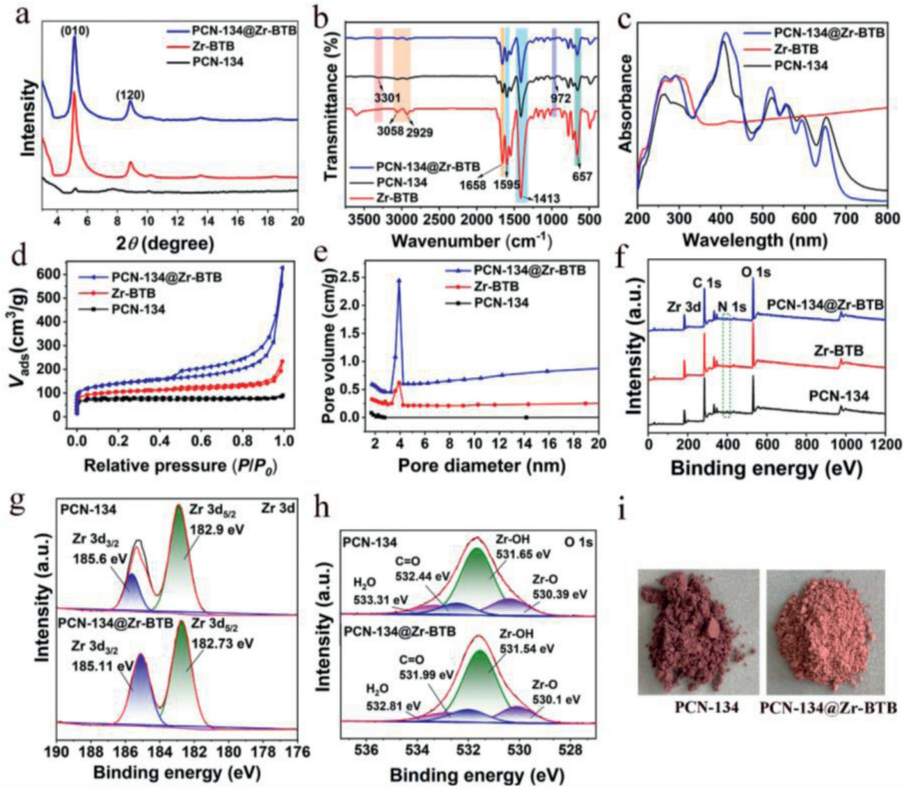

Fig. 2. PXRD patterns (a), FT-IR (b), UV–vis absorbance spectra (c), N_2 adsorption-desorption isotherms (d), Barrett-Joyner-Halenda (BJH) size distribution (e) and XPS survey (f) of PCN-134, Zr-BTB and PCN-134@Zr-BTB. High-resolution XPS of Zr 3d (g) and O 1s (h) of PCN-134 and PCN-134@Zr-BTB. (i) Photographs of PCN-134 and PCN-134@Zr-BTB.

tion samples [28–30]. In addition, the ultraviolet absorption spectra of those materials are shown in Fig. 2c. As shown in Fig. 2c, a blue-shifted characteristic peak for Zr-BTB and a red-shifted characteristic peak for PCN-134 were observed for their composite. The composite has both of characteristic peaks at the same time, which suggest the composite material contains both Zr-BTB and PCN-134. In addition, the porphyrin unit in the PCN-134@Zr-BTB exists in the form of TCPP, which can be proved by observing the four Q-bands in the UV spectrum [31]. N_2 adsorption and desorption isotherms and pore size distributions were performed to explore the specific surface area and porosity of those three materials (Figs. 2d and e). The Brunner-Emmett-Teller (BET) surface areas of PCN-134, Zr-BTB and PCN-134@Zr-BTB are 281, 388 and 501 m^2/g, respectively (Table S1 in Supporting information). The high specific surface area of PCN-134@Zr-BTB demonstrates that it combines the advantages of both the specific surface area of PCN-134 and the porosity of Zr-BTB, which facilitates the exposure of a great number of available adsorption sites on the surface. The N_2 adsorption-desorption isotherms of PCN-134@Zr-BTB exhibits a typical IV-type curves, which indicate its mesoporous feature (Fig. 2d), and the pore-size was 3.92 nm from Barrett-Joyner-Halenda (BJH) pore-diameter distribution curve (Fig. 2e).

The X-ray photoelectron spectroscopy (XPS) was employed to verify chemical composition and interactions of PCN-134@ZrBTB, and the results are displayed in Figs. 2f-h. The survey spectrum in Fig. 2f shows that Zr, C and O elements all existed in the three synthesized materials. The regional spectrum of N was observed in PCN-134 and PCN-134@Zr-BTB, which confirmed the existence of TCPP. As shown in Fig. 2g, the high resolution XPS spectrum of Zr 3d shows two peaks, which can be assigned to Zr-O bonds. Furthermore, in PCN-134@Zr-BTB, the binding energies of Zr 3d and O 1s bonds both shifted towards lower binding energy (Figs. 2g and h), which confirms the transfer of electrons from Zr-BTB to PCN-134 after composite. An obvious color change from dark brown to yellowish brown also confirmed the successful preparation of PCN-134@Zr-BTB composites (Fig. 2i).

The morphology of PCN-134 was determined by scanning electron microscopy (SEM), which revealed that the synthesized pure PCN-134 exhibits regular hexagonal sheets with distinct edges (Fig. 3a). The SEM and TEM images of PCN-134@Zr-BTB were shown in Figs. 3b-f. It can be observed that Zr-BTB nanosheets were evenly grown on the surface and edges of the PCN-134 nanoplates, forming a cactus-like morphology. The EDS analysis and elemental mapping images revealed that C, O, N and Zr elements were presented in PCN-134@Zr-BTB with uniform distribution (Fig. 3g and Fig. S5 in Supporting information). The adsorption peak areas and adsorption capacities of all materials including pure PCN-134, Zr-BTB-1.5, PCN-134@Zr-BTB and PCN-134/Zr-BTB for target BPs were also investigated and the results are presented in Figs. 3h and i. Obviously, PCN-134@Zr-BTB possessed the maximum adsorption peak areas and adsorption capacities for the four BPs. Thus, PCN-134@Zr-BTB was selected as sorbent of dispersive solid-phase extraction (dSPE) for further study.

The experimental parameters including amount of sorbent, adsorption time, pH of extraction solution, desorption time, type and volume of desorption solvent were systematically investigated using single-factor experiments to obtain the best extraction performance of PCN-134@Zr-BTB as dSPE sorbent. The detailed experimental processes as well as corresponding results, figures and tables (Figs. S6-S14 and Table S2 in Supporting information) were provided.

The quantitative parameters including linearity range, coefficient of determination (R^2), limits of detection (LODs) with signal-to-noise (S/N) at 3, limit of quantification (LOQs) (S/N = 10) and enrichment factor (EF) were investigated under optimal conditions to evaluate practicability of the proposed method. The data are presented in Table 1. Clearly, satisfactory linearity was observed for BPs in the range of 0.06–200 ng/mL with R^2 between 0.9979 and 0.9993. The LOQs ranged from 0.06 ng/mL to 0.08 ng/mL. The LODs of four BPs ranged from 0.02 ng/mL to 0.03 ng/mL. The EFs of BPs ranged from 310 to 374. The relative standard deviations (RSDs) of intra-day, inter-day, and batch-to-batch were in the ranges of 1.39%−4.11%, 4.09%−9.56% and 3.70%−7.94%, respectively. These results demonstrate that the synthesized PCN-134@Zr-BTB material has superior enrichment ability and good reproducibility.

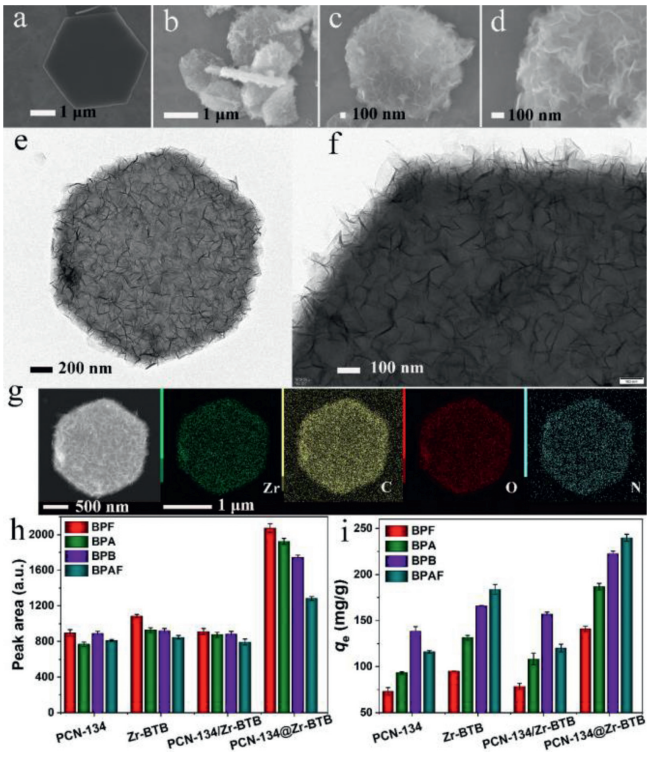

Fig. 3. SEM images of PCN-134 (a), and PCN-134@Zr-BTB (b-d). TEM images of PCN-134@Zr-BTB (e, f). Elemental mapping of PCN-134@Zr-BTB (g). The extraction performance (h) and adsorption capacities (q_e) (i) of PCN-134, Zr-BTB, physical mixing PCN-134/Zr-BTB, and PCN-134@Zr-BTB as sorbents for target BPs.

To further investigate the practical applicability of PCN-134@Zr-BTB material, the dSPE coupling with high performance liquid chromatography (HPLC) method was utilized to quantitatively analyze the trace contents of BPs in pond water and lake water. The results presented in Table 2 indicate that no target BPs were detected in pond water and BPAF was detected in the lake water with a concentration of 0.8 ng/mL. To investigate the accuracy of the proposed method, the recoveries were detected by spiking the real samples with three levels concentrations (1, 10 and 100 ng/mL) of BPs standard solutions, and then analyzing the spiked samples by the present PCN-134@Zr-BTB-dSPE-HPLC method. As listed in Table S4 (Supporting information), the recoveries ranged from 72.8% to 103% and from 83.0% to 112.7% for pond water and lake water with RSDs ($n = 3$) of 3.24%−10.9% and 1.05%−12.7%, respectively. In addition, Fig. S15 (Supporting information) presents the representative chromatograms of lake water sample. To provide retention time as a reference, the chromatograms of 5 μg/mL mixed standard solution analyzed directly by HPLC are shown in Fig. S15d. In addition, Figs. S15a and b present the chromatograms of the lake water samples before and after enrichment with PCN-134@Zr-BTB adsorbents, respectively. Fig. S15c shows the chromatogram of spiked lake water sample after enrichment with the adsorbents. All these results demonstrated that the developed PCN-134@Zr-BTB-

Table 1
Analytical parameters of PCN-134@Zr-BTB for HPLC-DAD determination of BPs.

Analytes	Linear range (ng/mL)	R^2	LODs (ng/mL)	LOQs (ng/mL)	EFs	Repeatability, (RSD, %) ($n = 3$)		
						Intra-day	Inter-day	Batch-to-batch
BPF	0.08–200	0.9993	0.03	0.08	310	1.39	5.33	7.94
BPA	0.06–200	0.9984	0.02	0.06	324	2.88	4.09	3.70
BPB	0.06–200	0.9979	0.02	0.06	323	2.24	6.17	3.67
BPAF	0.08–200	0.9989	0.03	0.08	374	4.11	9.56	6.58

Table 2
The recoveries of BPs in real water samples.

Samples	Analytes	Found (ng/mL)	1 (ng/mL)		10 (ng/mL)		100 (ng/mL)	
			Recovery (%)	RSD ($n = 3$, %)	Recovery (%)	RSD ($n = 3$, %)	Recovery (%)	RSD ($n = 3$, %)
Pond water	BPF	N.D.	72.8–89.4	8.92	83.5–94.8	5.76	89.9–98.6	4.75
	BPA	N.D.	74.9–96.7	10.9	76.6–84.2	3.78	89.3–96.3	3.54
	BPB	N.D.	79.4–95	8.68	83.3–97.4	7.05	92.2–98.7	3.24
	BPAF	N.D.	73.8–93.1	9.75	88.2–97.1	6.88	93.1–103	5.43
Lake water	BPF	N.D.	85.7–112.7	12.7	89.5–97.6	6.12	89.0–95.1	4.69
	BPA	N.D.	83.0–98.1	11.7	88.9–102	7.30	101.7–108	4.99
	BPB	N.D.	87.7–98.7	8.35	95.1–104	6.32	99.1–105.6	4.49
	BPAF	0.8	84.2–97.4	10.3	96.3–101	3.37	99.7–101.2	1.05

Note: N.D. represents not detected.

dSPE-HPLC method can satisfied the detection of trace BPs in real water samples with good applicability and reliability.

The reusability of sorbents has great significance in practical applications. To evaluate the reusability of PCN-134@Zr-BTB, the reusability experiments of adsorbed BPs were carried out and the result are shown in Fig. S16a (Supporting information). The results displayed that the extraction ability of PCN-134@Zr-BTB showed no pronounced decrease over the repeated seven cycles. In addition, PCN-134@Zr-BTB after the seventh cycle was also characterized by XRD (Fig. S16b in Supporting information). The XRD of PCN-134@Zr-BTB had no significant phase change compared with the newly synthesized sorbent material. Meanwhile, the stability of PCN-134@Zr-BTB was also investigated. To investigate its stability, PCN-134@Zr-BTB was immersed in aqueous solution at pH 2, 5 and 10 as well as in acetonitrile for 48 h, respectively. The XRD (Fig. S16c in Supporting information) demonstrated that the sample had no significant phase change. Meanwhile, PCN-134@Zr-BTB sample were immersed in aqueous solutions from pH 2 to pH 11 for 48 h. Then the mass of Zr dissolution were determined by ICP-AES (Fig. S16d in Supporting information). The concentration of Zr^{4+} was 0.225 mg/L after immersion in an aqueous solution at pH 2 for 48 h, which corresponds to 20 mg PCN-134@Zr-BTB sorbent loss of 1.35 μg. And between pH 3 and pH 11, the loss of Zr is less than 0.6 μg, which can be negligible. All the results indicated that the PCN-134@Zr-BTB material has superior stability and reusability.

Then, to explore the adsorption behavior of target BPs onto the sorbent, adsorption isotherms and adsorption kinetics models were adapted to fit the experimental data. The equations of those models were shown in Supporting information. Fig. 4a shows the adsorption amounts of four target BPs at different initial concentrations. Figs. 4b and c present the adsorption experimental data fitted with the Langmuir and Freundlich models, respectively. The relevant parameters obtained from the above two models are summarized in Table S3 (Supporting information). As illustrated in Table S3, for all target BPs, the R^2 of Langmuir isotherm model (0.9993–0.9997) were all better than that of Freundlich isotherm model (0.9162–0.9677). These results demonstrated that the adsorption of BPs onto PCN-134@Zr-BTB was consistent with the Langmuir model. According to the Langmuir equation, the maximum adsorption amounts of four BPs were in the range of 135.1–628.9 mg/g, indicating that PCN-134@Zr-BTB is a promising sorbent for adsorption and extraction of BPs. Figs. 4d and e show that PCN-134@Zr-BTB can rapidly adsorb BPs within 10 min and reach the adsorption equilibrium state in about 20 min. The equilibrium adsorption amounts of four BPs were in the range of 87.4–319.5 mg/g. Meanwhile, the adsorption rates of the examined BPs on the adsorbents were in the order of BPAF (99.8%) > BPB (99.6%) > BPA (95.5%) > BPF (85.5%). This rapid kinetics and different adsorption rates may be attributed to the strong affinity between the BPs and -OH groups on the PCN-134@Zr-BTB adsorbent [32].

Four kinetic models, *pseudo*-first-order (Fig. 4f), *pseudo*-second-order (Fig. 4g), intra-particle diffusion (Fig. 4h) and liquid-film diffusion (Fig. 4i) models were utilized to fit the experimental data. The kinetic parameters and correlation coefficient (R^2) were displayed in Table S4 (Supporting information). The best fitted kinetic model was assessed depending on the correlation coefficient (R^2) values. As seen in Table S4, the R^2 of *pseudo*-second-order kinetic model (0.9996–0.9997) were all higher than those of *pseudo*-first-order kinetic model (0.9148–0.9932). Also, the adsorption capacity ($q_{e,\,cal}$) acquired by *pseudo*-second-order kinetic model were much closer to the experimental values ($q_{e,\,exp}$). Therefore, the adsorption of BPs on PCN-134@Zr-BTB adheres to the *pseudo*-second-order kinetic model. As shown in Fig. 4h and Table S4. The intra-particle diffusion model shows three distinct linear regions, which indicates that the complete adsorption kinetic process contains three stages, *i.e.*, external surface adsorption, intra-particle diffusion and adsorptive attachment, respectively [33,34]. The adsorption rate constants of three stages were in the order of $k_i > k_{ii} > k_{iii}$, indicating a gradual slowing down of the adsorption rate in these three stages. Meanwhile, the rate constants of first and second stages are relatively high, indicate the presence of external surface adsorption and intra-particle diffusion. The last stage was the adsorption equilibrium. Moreover, the multilinear plots were not through the origin ($C \neq 0$), indicating that the sorption-limiting step was not only controlled by intra-particle diffusion [35,36]. The liquid-film diffusion model also fitted the experimental data well (Fig. 4i and Table S4), indicating that both intra-particle diffusion and liquid-film diffusion influence the adsorption process together. All the above results suggest that the adsorption mechanism is a combination of physical and chemical adsorption, while chemisorption is the main step in controlling the rate.

Based on the effect of pH, adsorption isotherms and adsorption kinetics on the adsorption capacity and extraction efficiency

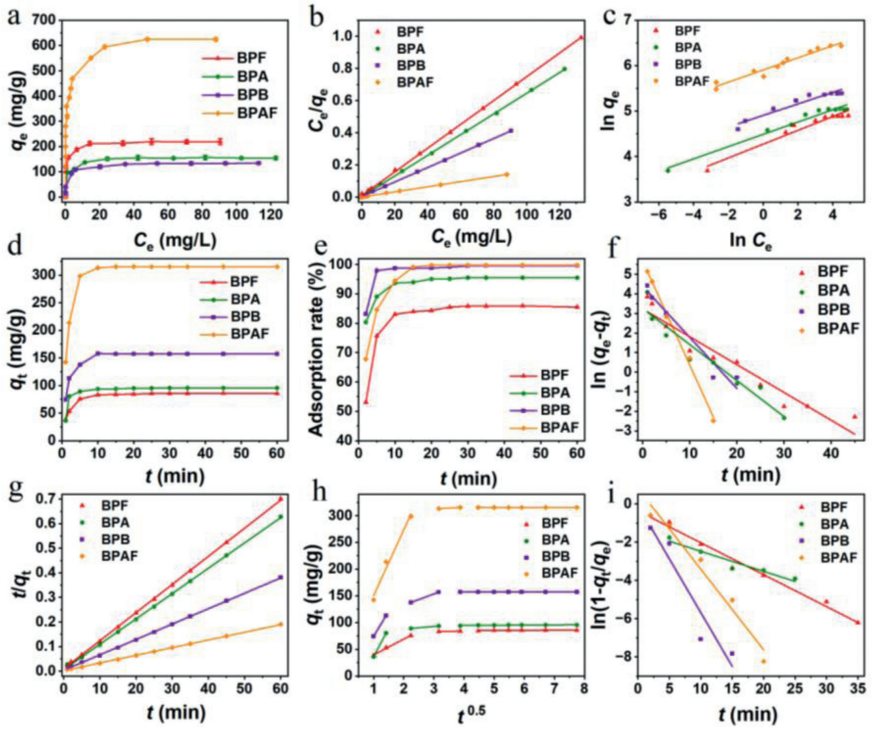

Fig. 4. Adsorption isotherms (a), Langmuir model (b), Freundlich model (c), adsorption kinetics (d), *pseudo*-first-order model (e), *pseudo*-second-order model (f), adsorption rate (g), intra-particle diffusion model (h) and liquid-film diffusion model (i) of BPs on the PCN-134@Zr-BTB material.

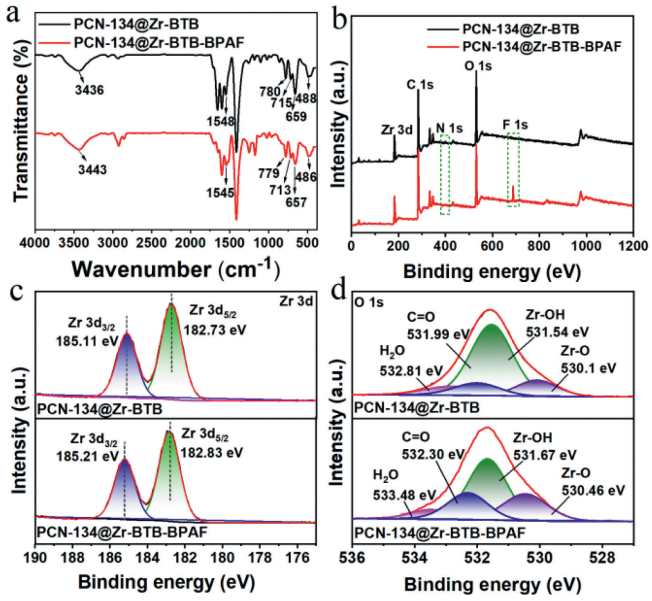

Fig. 5. FT-IR (a), XPS survey (b), high-resolution XPS of Zr 3d (c) and O 1s (d) of PCN-134@Zr-BTB before and after adsorption of BPAF.

of BPs in the above experiments, it can be concluded that hydrogen bonding and π-π stacking may be the most important adsorption mechanism. In order to further elucidate the adsorption mechanism of BPs on sorbent, the PCN-134@Zr-BTB sample before and after adsorption of BPAF were analyzed by XPS and FT-IR. Fig. 5a shows the FT-IR spectra of PCN-134@Zr-BTB before and after adsorption of BPAF. After BPAF adsorption, the FT-IR peaks of the -OH group shifted from 3436 cm^{-1} to 3443 cm^{-1}, which indicates the presence of H-bonding interactions. A shift in the peak of aromatic C=C group from 1557 cm^{-1} to 1550 cm^{-1} was also remarked, suggesting the possibility of π-π stacking. Meanwhile, the broad band (478–800 cm^{-1}) of the deformation vibration attributed to Zr-OH is slightly shifted. This may be attributed to the formation of hydrogen bonds between the sorbent and BPs molecules [37]. Fig. 5b shows the XPS analysis of PCN-134@Zr-BTB before and after adsorption of BPAF. It was found that they both have Zr 3d, N 1s, C 1s and O 1s, while F 1s as a new peak only appeared in PCN-134@Zr-BTB-BPAF, which indicating BPAF was successfully adsorbed on the PCN-134@Zr-BTB. The Zr 3d spectra of PCN-134@Zr-BTB and PCN-134@Zr-BTB-BPAF were displayed in Fig. 5c. As for PCN-134@Zr-BTB, the peaks of Zr $3d_{3/2}$ and Zr $3d_{5/2}$ were located at 185.11 and 182.73 eV, respectively. However, after adsorbing BPAF, the peaks of Zr $3d_{3/2}$ and Zr $3d_{5/2}$ shifted to a higher binding energy by about 0.1 eV at 185.21 and 182.83 eV, respectively. This may be attributed to the zirconium electron density loss due to binding to fluorine in BPAF, which conversely increases the binding energy of Zr $3d_{3/2}$ and Zr $3d_{5/2}$ peaks [38]. The O 1s spectra of PCN-134@Zr-BTB and PCN-134@Zr-BTB-BPAF are shown in Fig. 5d. Every spectrum was divided into four peaks at 530.1 (Zr-O), 531.54 (Zr-OH), 531.99 (C=O) and 533.48 eV (H_2O), respectively [39]. After adsorption of BPAF, the area ratio of Zr-OH peak decreased from 63.9% to 47.66%, respectively. This result suggested the formation of hydrogen bonds between sorbent and BPAF molecules. Based on FT-IR and XPS analysis, the adsorption of BPs molecules on PCN-134@Zr-BTB sorbent is mainly through hydrogen bonding and π-π stacking.

The selectivity of PCN-134@Zr-BTB sorbent was investigated using BPAF, BPF, acenaphthene (ANE), phenanthrene (PHE), and estrogens (estrone, E1; hexestrol, HEX; and 17α-estradiol, 17α-E2) as analytes, as shown in Table S5 (Supporting information). PCN-134@Zr-BTB exhibited a favorable extraction effect on BPAF and BPF with EF values higher than 258, further implying the essential effect of hydrogen bonding and π-π stacking between BPs and PCN-134@Zr-BTB. However, the EF value of PCN-134@Zr-BTB for BPF (EF = 258) was lower than that of BPAF (EF = 317), which may be attributed to that the reduction of C-F bonding in BPF, resulting

in less hydrogen bonding interactions. The EF values of ANE and PHE were 9.92 and 15.02, respectively, which were due to the weak π-π stacking interaction between ANE, PHE and PCN-134@Zr-BTB. Meanwhile, the EF values of estrogens were all higher than 135.7, indicating that PCN-134@Zr-BTB also had a good adsorption effect on estrogens. This was because hydrogen bonds and π-π stacking can also be formed between PCN-134@Zr-BTB and estrogens. All these results showed that the PCN-134@Zr-BTB as sorbent can selectivity adsorb some compounds that can form hydrogen bonds and π-π stacking interaction.

To further evaluate the performance of the established PCN-134@Zr-BTB-dSPE method, which was compared with other reported methods. As observed in Table S6 (Supporting information), the method had a relatively wide linear range, a low detection limit and a significantly higher enrichment factors than other literatures. The maximum adsorption capacity of PCN-134@Zr-BTB as sorbent for BPs was compared with other literatures (Table S7 in Supporting information). It can be seen that the adsorption capacities of PCN-134@Zr-BTB for BPs are higher than that of other sorbents. The results imply that PCN-134@Zr-BTB was an ideal sorbent material for removal and enrichment of BPs from environmental water.

In conclusion, a new strategy to control the selective growth of 2D-MOF (Zr-BTB) nanosheets on the surface and edges of 3D-MOF (PCN-134) nanoplates was proposed to prepare cactus-like PCN-134@Zr-BTB material. Compared to pure PCN-134 and Zr-BTB-1.5 materials, PCN-134@Zr-BTB-1.5 delivers the highest adsorption capacity and extraction efficiency. The adsorption process of PCN-134@Zr-BTB material can be better described by Langmuir isotherm model and *pseudo*-second-order model in this case. Meanwhile, both intra-particle diffusion and liquid-film diffusion models fitted the experimental data well, demonstrating that the adsorption was mainly dominated by physical adsorption through π-π stacking and chemisorption through hydrogen bond formation. The fabricated PCN-134@Zr-BTB material displayed a relatively high adsorption capacity (135.1–628.9 mg/g) with good reusability and stability. It provided an opportunity for the synthesis of new MOF@MOF materials from 2D-MOF nanosheets and application as adsorbents for the adsorption of bisphenol contaminants in environmental water.

Declaration of competing interest

The authors declare that they have no known competing financial interests or personal relationships that could have appeared to influence the work reported in this paper.

Acknowledgments

This work was sponsored by National Natural Science Foundation of China (No. 22076038), Natural Science Foundation of Henan Province, China (No. 202300410044), and Henan Key Scientific Research Programs to Universities and Colleges (No. 22ZX003).

Supplementary materials

Supplementary material associated with this article can be found, in the online version, at doi:10.1016/j.cclet.2023.108620.

References

[1] Z. Zhang, X. Huang, J. Ma, et al., Water Res. 201 (2021) 117288.
[2] L. Han, X. Zhang, D. Li, et al., Talanta 235 (2021) 122818.
[3] X. Wei, Y. Hu, Q. Zhu, et al., Environ. Res. 204 (2022) 112366.
[4] J. Li, W. Zhang, Y. Zhou, et al., Environ. Pollut. 270 (2021) 116044.
[5] J. Peng, Y. He, C. Zhou, S. Su, B. Lai, Chin. Chem. Lett. 32 (2021) 1626–1636.
[6] H. Zhang, G. Li, Q. Zhu, et al., J. Hazard. Mater. 439 (2022) 129584.
[7] X. Zhang, D. Li, M. Li, et al., Chem. Eng. J. 448 (2022) 137467.
[8] X. Wang, X. Cui, H. Ji, et al., Chin. Chem. Lett. 32 (2021) 3199–3201.
[9] Y. Wu, H. Chen, Y. Chen, et al., Sci. China Chem. 65 (2022) 650–677.
[10] L. Han, P. Qin, M. Li, Chem. Eng. J. 456 (2023) 140969.
[11] W. Gao, M. Li, Y. Fa, et al., Chin. Chem. Lett. 33 (2022) 3849–3852.
[12] M. Zhang, X. Yan, W. Ma, et al., Talanta 221 (2021) 121651.
[13] B. Zhao, L. Jiang, Q. Jia, Chin. Chem. Lett. 33 (2022) 11–21.
[14] M. Li, X. Ren, Y. Gao, et al., Chem. Commun. 58 (2022) 7574–7577.
[15] X. Zhang, Y. Yang, P. Qin, et al., Chin. Chem. Lett. 33 (2022) 903–906.
[16] W.Q. Tang, Y.J. Zhao, M. Xu, et al., Angew. Chem. Int. Ed. 60 (2021) 6920–6925.
[17] J.M. Park, S.H. Jhung, Chem. Eng. J. 396 (2020) 125224.
[18] L. Han, X. Liu, X. Zhang, et al., J. Hazard. Mater. 424 (2022) 127559.
[19] Y. Yuan, X. Zheng, H. Lin, et al., Talanta 211 (2020) 120713.
[20] O.K. Farha, I. Eryazici, N.C. Jeong, et al., J. Am. Chem. Soc. 134 (2012) 15016–15021.
[21] Y. Qin, Y. Wan, J. Guo, M. Zhao, Chin. Chem. Lett. 33 (2022) 693–702.
[22] X. Shi, H. Xu, Y. Wu, J. Anal. Test. 5 (2021) 165–173.
[23] M. Zhao, Y. Huang, Y. Peng, et al., Chem. Soc. Rev. 47 (2018) 6267.
[24] M. Zhao, J. Chen, B. Chen, et al., J. Am. Chem. Soc. 142 (2020) 8953–8961.
[25] M. Liu, Y. Liu, X. Liu, et al., Chin. Chem. Lett. 34 (2023) 107708.
[26] Y. Gao, J. Xia, D. Liu, et al., Chem. Eng. J. 378 (2019) 122118.
[27] Y. Wang, L. Feng, J. Pang, et al., Adv. Sci. 6 (2019) 1802059.
[28] S. Yuan, J.S. Qin, L. Zou, et al., J. Am. Chem. Soc. 138 (2016) 6636–6642.
[29] H. Huang, Z. Fang, R. Wang, et al., Small 18 (2022) 2200407.
[30] Y. Zong, S. Ma, J. Gao, et al., ACS Omega 6 (2021) 17228–17238.
[31] J. Chen, H. Chen, T. Wang, et al., Anal. Chem. 91 (2019) 4331–4336.
[32] L. Li, D. Xu, Z. Pei, RSC Adv. 6 (2016) 60145–60151.
[33] M. Qin, Y. Shi, D. Lu, et al., Appl. Surf. Sci. 595 (2022) 153494.
[34] R.M. Abdelhameed, H.E. Emam, Sustain. Mater. Techno. 31 (2022) e00366.
[35] P. Qin, D. Chen, D. Li, et al., Food Chem 409 (2023) 135272.
[36] H.E. Emam, R.M. Abdelhameed, H.B. Ahmed, J. Environ. Chem. Eng. 8 (2020) 104386.
[37] G. Li, X. Zhang, J. Sun, et al., J. Hazard. Mater. 381 (2020) 120985.
[38] J. He, X. Cai, K. Chen, et al., J. Colloid Interf. Sci. 484 (2016) 162–172.
[39] J. Wang, W. Xu, L. Chen, et al., Chem. Eng. J. 231 (2013) 198–205.